4.4 Injection System

4.4.1 Electron Source

4.4.1.1 Polarized Gun

At present, all operating polarized electron sources are using DC-guns generating long pulses in the ns range, usually followed by a bunching system (see e.g. [1]). A GaAs cathode is illuminated by suitable laser pulses to extract pulses of polarized electrons.

An injection system, which meets the requirements for SBLC is being built at the S-Band Test Facility. It uses a pulsed DC-gun operating at 90 kV. The following discussion is based on a gun with similar performances.

Space charge and cathode charge limit Space charge limits the extractable current of a DC-gun. The limit can be estimated using Child-Langmuir's law. The 90 kV gun has a perveance of $0.23\,\mu A/V^{3/2}$, limiting the current to 6 A.

A more severe limitation specific to GaAs-type cathodes is the so called cathode charge limit [2]. This limitation is typical for semiconductor cathodes with a negative electron affinity (NEA) surface, where a high electron extraction probability is achieved by the application of alkalis and oxides to the surface of the GaAs crystal. The NEA surface (together with the p-dopant, which bends the energy bands downwards at the surface) lowers the vacuum level below the conduction band minimum in the bulk, resulting in high extraction rates. The limit can be understood as a competition between the rate of near-thermal electrons arriving from the conduction band at the surface and the discharge rate of electrons from the surface [3].

The cathode charge limit can be estimated using SLC data [4]: the SLC gun produces about 10 nC in a 2 ns long pulse from a cathode of an area of $1.5\,cm^2$ close to the cathode charge limit. A 100 nm medium-doped ($5{\cdot}10^{18}/cm^3$) strained-lattice GaAs cathode layer is used. The acceleration voltage is 1.8 MV/m. Thus, the charge density is limited to $7\,nC/cm^2$.

Since the current density scales linearly with the acceleration voltage E [5], the charge density on the cathode will be limited to $8\,nC/cm^2$ for a field at the cathode of 2 MV/m. With a cathode area of $2\,cm^2$, the extractable charge is about 16 nC well above the SBLC requirements.

The charge limit is experimentally verified for bunch lengths in the order of ns. Conservatively, one may assume that the charge density limit turns into a current density limit already for bunches as short as 0.3 ns [6]. With this assumption, the current will be limited to $3.7\,A/cm^2$ for the SBLC gun. To extract bunches of 2 nC from the $2\,cm^2$ cathode, the bunch length must exceed 300 ps.

Shorter bunch lengths are preferred, since it would simplify the bunching system. This can be achieved by increasing the acceleration voltage or by using a larger cathode. On the other hand, to avoid damaging the cathode by ion bombardment, the dark current should be kept as low as possible. Besides a careful processing of the gun this requires low fields at the electrodes. The SLC gun operates at 120 kV with a dark current of less than 50 nA. The highest field on the electrodes is 7 MV/m [1].

Multi bunch operation For multi bunch operation, an additional effect of the cathode charge limit gets important: the temporary flattening of the bands in the band bending region due to trapped electrons in the surface states, preventing further electrons from being extracted. Experiments at the SLC have shown, that the recovery time of the cathode is in the order of 10 to 100 ns depending on the cathode thickness [1]. Using a highly doped, thin cathode ($2{\cdot}10^{19}/\mathrm{cm}^3$, 100 nm), a reduction of the charge of the second bunch is expected to be only 10 % for bunch to bunch separation of 6 ns. For the following bunches, a steady state at a reduced charge will build up.

Polarization, quantum efficiency and lifetime A polarized electron beam is produced by applying circular polarized laser light on a strained lattice GaAs cathode. SLC data show a polarization maximum of more than 80 % at a laser wavelength of 845±10 nm [7]. Unfortunately, the quantum efficiency drops sharply for highest polarization to 0.1 ... 0.3 %. In addition, the quantum efficiency depends strongly on the operating conditions of the gun. High dark current of more than 50 nA and poor vacuum conditions reduces the quantum efficiency significantly. The vacuum must be maintained below $1{\cdot}10^{-11}$ mbar. In addition, activation of the cathode by cesiation is regularly required. To obtain a reasonable up time of the source, a loading system which enables loading and removal of the cathode without breaking the gun vacuum is essential. Conditioning of the gun, regular cesiation and other cathode manipulations will be done with the cathode removed. A transport chamber will allow to insert a cathode prepared in a separate preparation chamber.

SLC is operating their gun with the same cathode for more than a year with a quantum efficiency between 0.1 and 0.3 % at highest polarization. The regular cesiation required to maintain this efficiency is done in situ without breaking the vacuum [7].

Laser Most polarized electron sources use lasers based on Ti:Sapphire, which are commercially available, especially for cw and pulsed applications with low repetition rates of a few tens of Hz. These lasers are tunable in a wide range around 800 nm and exceed easily the power or pulse energy requirements for most sources.

The laser may consist of Ti:Sapphire oscillator producing a long pulse of 2 μs with an energy of 1 mJ. It is pumped by a Nd:YAG laser system running at 50 Hz. The long pulse is sliced into 333 short pulses with a distance of 6 ns between the pulses and a length of 1 ns or shorter if required using resonant Pockels cells. It is also possible, to generate the pulse train directly in a pulse train oscillator running at 167 MHz. The pulse train will be amplified by a Ti:Sapphire power amplifier to 50 μJ per pulse. On the cathode, about 10 μJ are required to produce an electron bunch of 3 nC. An extensive feedback system is used to stabilize the pulse energy and phase.

4.4.1.2 Injector Linac

This section explains the conventional electron injector and pre-linac. The injector linac is composed of two main parts. It starts with the injector consisting of the electron source and a bunching system followed by the linac part responsible for accelerating

		SBTF			SBLC
ν_t, train repetition frequency	$[Hz]$	50			
I_t, average current in train	$[mA]$	300			
T_t, length of train	$[\mu s]$	2			
bunchlength at injector exit		$\leq 16^\circ_{3GHz}$			
energy at injector exit		$E_{kin} \geq 3\,MeV$			
T_{bb}, bunch to bunch separation	$[ns]$	24	16	8	6
n_t, bunches per train		83	125	250	333
q_b, charge per bunch	$[nC]$	7.2	4.8	2.4	1.8
ν_{SHB1}, frequency of 1. SHB	$[MHz]$	125			166
length of gunpulse	$[ns]$	$\approx 2.0 - 2.5$			$\approx 1.5 - 2.0$
gun peak current	$[A]$	≈ 6			≈ 2

Table 4.4.1: *Comparison between required injector parameters for SBTF and SBLC operation.*

the beam up to the damping ring energy of $3\,GeV$. Determined by the longitudinal and transverse acceptance of the damping ring, upper limits for the energy spread and the normalized emittance at the end of the injector linac are $\Delta E/E \leq 1\,\%$ and $\epsilon_n^{rms} \leq 1 \cdot 10^2\,\pi\,mm\,mrad$, respectively. The time structure and bunch population are given by the collider parameters. Based on a $\nu_t = 50\,Hz$ repetition rate $T_t = 2\,\mu s$ long bunchtrains with an average current of $I_t = 300\,mA$ are required. Being separated by $\Delta t_b = 6\,ns$ each of the 333 single bunches in one train carries a charge of $q_b = 1.8\,nC$ equivalent to a bunch population of $N_b = 1.125 \cdot 10^{10} e^-$. The accelerating part of the injector linac will consist of an S-band linac adopting the same technique as proposed for the SBLC main linac. For $3\,GeV$ roughly 31 regular $6\,m$ long accelerating structures ($\beta = 1$, $2\pi/3$ – mode, $17 MV/m$) intersected by focussing quadrupoles are needed, i.e. an overall accelerator length of about $200\,m$. One $150\,MW\,/\,3\,\mu s$ S-band klystron supplies two $6\,m$ structures. Applying the same scheme of beamloading compensation as in the main linac the energy spread at the end of the linac is dominated by the bunchlength at its entrance. To obtain $\Delta E/E \leq 1\,\%$ the injector has to deliver bunches of a length less than $16^\circ_{3GHz} = 14.8\,ps$ in time corresponding to a length of $4.4\,mm$ if the beam is relativistic. In that case the injector is fully responsible for the bunching and the first accelerating section takes over a bunch which longitudinal dynamics is already frozen. The clear-cut between bunching and acceleration guarantees an independant operation of the injector and accelerating sections. For this reason the beam should leave the injector with a kinetic energy of $E_{kin} \geq 3\,MeV \Leftrightarrow \beta \geq 0.9$. Since the damping ring acceptance is large the emittance constraint on the injector part is relaxed and does not represent a severe problem.

Except for the bunch spacing Δt_b the design of the injector for the S-Band Test Facility (SBTF) is based on the same parameters. For the purpose of wakefield related studies the bunch spacing Δt_b can be varied between $8\,ns$, $16\,ns$ or $24\,ns$ in the SBTF. Keeping the average current within the bunchtrain at $I_t = 300\,mA$ results in a maximum bunchcharge of $7.2\,nC$ in the last case. Table 4.4.1 compares the injector requirements for the SBTF and the SBLC. Having found a reasonable concept for the SBTF injector there is no doubt that an injector for the SBLC can be realized in the same manner, since the operation conditions are more relaxed in terms of bunchcharge. Thus the following paragraphs are going to present the performance of the SBTF injector as derived from EGUN or PARMELA calculations as well as has been measured at the existing part of it. Requiring multibunch operation in combination with high bunchcharge a conventional scheme as sketched in Fig. 4.4.1 based on a thermionic gun with a gridded cathode followed by a bunching system using two subharmonic (SHB1 and SHB2) and two fundamental bunchers (TWB1 and TWB2) was decided for. The impact of the deviating SBLC requirements on the presented layout for the SBTF injector will be discussed at the relevant design steps.

Electron Source Production of $2\,\mu s$ long bunchtrains with $300\,mA$ average current is required. The current the gun has to deliver is determined by the length of the gunpulse and its charge. For clean capture at SHB1 the gunpulse should have a length in the order of a quarter of its period time. In order to relax the requirements on the gun the frequency of the subharmonic buncher SHB1 has to be as low as possible, but nevertheless has to match with the time structure of the bunchtrain. That is why SHB1 runs at $125\,MHz$ in SBTF respectively needs to be $166\,MHz$ at SBLC, which implies a gunpulse length of about $FWHM \approx 2\,ns$ respectively $FWHM \approx 1.5\,ns$. For SBTF operation the maximum charge including a $60\,\%$ safety margin has to be $12\,nC = 7.5 \cdot 10^{10} e^-$ resulting in a gun current of $6\,A$. For SBLC parameters the situation is more relaxed. The required guncharge is only $3\,nC$, i.e. less by a factor of 4 and its current reduces by a factor of 3 down to $2\,A$ due to the shorter pulse length.

The gunvoltage of $90\,kV$(dc) has been chosen as low as possible in order to simplify the process of bunching and keeping the SHB amplitudes at moderate levels. On the other hand as shown by PARMELA calculations this value is high enough to tolerate spacecharge effects (bunchlengthening and energy modulation) in the $75\,cm$ long drift up to SHB1. Based on the EIMAC Y796 cathode grid assembly, which emits from a circular cathode area of $2\,cm^2$ (equivalent to $8\,mm$ in radius) a gun geometry was modelled by means of EGUN simulation. The result is shown in Fig. 4.4.2. With a $34\,mm$ anode cathode gap this gun has a calculated perveance of $0.22\,\mu A/V^{1.5}$. At $90\,kV$ this is equivalent to $6\,A$ space charge limited current, which was experimentally proven when driving it with single pulses of a few μs in length.

Extraction of bunchtrains consisting of short pulses is achieved by means of a special pulser that is housed inside the $240\,mm$ long gun ceramic close to the gun cathode. In combination with a high bandwidth optical transmission and amplifier system the pulser input is supplied with $2\,ns$ wide pulses of $60\,V$ peak and the desired time structure. The gunpulser amplifies these pulses by means of a three stage triode circuit interconnected by ferrite loaded coaxial transformers in which the third triode with its anode directly connected to the guncathode operates in a current source mode. Measured at $31.6\,cm$ behind the gun at wall current monitor CM1 Fig. 4.4.3 shows the beampulses having a FWHM-length of typically $2.2\,ns$, a subnanosecond risetime and a peak current of up to $4.5\,A$, which is less than the gun capability since it is limited by the current output of the last triode stage. Due to a saturation effect of the interstage transformer cores we observe a drop down from $10\,nC$ in the first pulse to a $70\,\%$ equilibrium level within the first 3 pulses of a $2\,\mu s$ bunchtrain with 250 pulses in $8\,ns$ mode. Although reduced down to $7\,nC$ this bunchcharge is by a factor of 2.9 well beyond the required $2.4\,nC$ for $8\,ns$ operation. Except for the first 3 pulses the intensity stability is better than $4\,\%$ over the whole bunchtrain.

This scheme of bunchtrain production has been sucessfully commissioned and fulfills all the requirements in terms of time structure, bunchcharge as well as stability in intensity and timing [9]. Since the intensity requirements are more relaxed for SBLC this scheme might even work at $6\,ns$ operation but has not been tested yet. If not applicable a resonant driving circuit for the gun can be used alternatively.

Bunching System Starting with the EGUN calculated transverse beam parameters at the gun exit a $90\,kV\,/\,12\,nC$ pulse with a length of $FWHM = 2.5\,ns$ ($FW = 3.0\,ns$) was used as an input to PARMELA calculations in order to optimize the process of bunching and lead to a layout as shown in Fig. 4.4.1 [8].

Starting with $z = 0$ at the gun anode a $125\,MHz$ cavity (SHB1) with a $30\,mm$ wide gap is located at $z = 75\,cm$. Running at an amplitude of about $34\,kV$ more than $80\,\%$ of the initial charge can be found in $120°$ of $500\,MHz$ at a distance of $116\,cm$ downstream of SHB1. Therefore a second cavity SHB2 with a gap of $40\,mm$ running at $500\,MHz$ is centered at $z = 191\,cm$. The optimum longitudinal focal point appears already $24\,cm$ behind the SHB2 gapcenter at $z = 215\,cm$. At this position PARMELA predicts a bunchlength of $FWHM \approx 0.19\,ns$ equivalent to about $200°$ of S-band. Measurements at that position show a bunchlength of $300\,ps$ with a transmission of $85\,\%$ when starting with a typical gunpulse ($2.2\,ns\,/\,4.5\,A$) of $10\,nC$ [10]. Unfortunately this measurement was bandwidth limited by the wallcurrent monitor and thus represents an upper limit for the true bunchlength. Without further measures the mentioned transmission and bunching results are only valid for the first pulses in the bunchtrain, since the following ones are heavily affected by amplitude and phase changes in the cavities due to beamloading. Made from stainless steel both cavities have a $Q_0 \approx 2700$ and a R/Q about $82\,\Omega$ respectively $101\,\Omega$. They are powered by a $10\,kW\,/\,20\,\mu s$ pulsed RF transmitter each. Neglecting its decay the beam induced voltage ($U = \omega \cdot R/Q \cdot q$) after half of the $2\,\mu s$ bunchtrain with $300\,mA$ has passed the cavities is $19\,kV$ in SHB1 and $95\,kV$ in SHB2. By means of a feedforward system acting on the amplitude and phase control circuits of both transmitters it is possible to obtain similar amplitude and phase conditions for every bunch of the train when entering the cavity.

Being still too long for the linac the bunches continue the process of longitudinal compression when entering a 4-cell S-band travelling wave structure (TWB1) having its first cellcenter at $z = 215\,cm$. TWB1 operates in $2\pi/3$-mode, has a phase velocity of $\beta = 0.6$ and is expected to run with a gradient of $7\,MV/m$. TWB1 is followed by a 16-cell, $\beta = 0.95$, $8\pi/9$-mode S-band travelling wave buncher (TWB2) running at

$12\,MV/m$ and being separated from TWB1 by only $9\,cm$ when measuring the distance between the last cellcenter of TWB1 and the first cellcenter of TWB2. The $8\pi/9$-mode was chosen to reduce the group velocity in order to relax the power requirement on the feeding klystron. Looking roughly $70\,cm$ downstream of TWB2 simulations predict a bunchlength of less than $10\,ps$, which has not been experimentally proven yet since the hardware is not commissioned up to this point. Simultaneously both TWB's accelerate the beam up to about $4\,MeV$. Therefore a short relativistic bunch enters the first regular accelerating section at $z = 360\,cm$.

When used as an injector for the injector linac at SBLC the same bunching system can be applied except that SHB1 has to be replaced by a $166\,MHz$ cavity and the distance between SHB1 and SHB2 may be optimized. Beamloading effects are identical because the average current in the bunchtrain remains the same.

Transverse Dynamics Up to SHB2 the free aperture of the beampipe has a diameter of $34\,mm$. While getting shorter, the beampulses are transversely focussed by means of a longitudinal magnetic field B_z created by distributed solenoids AF4 to AF27. At the guncathode B_z is set to zero with the help of bucking coil AF1. With two matching solenoids AF2 and AF3 the beamsize is adjusted to fill about $70\,\%$ of the beampipe, because a large ratio reduces spacecharge effects, and is tried to be kept constant up to SHB2. With a level around $100\,Gauss$ around SHB1 B_z slowly increases more or less according to the law of a Brillouin fieldstrength. Just before entering TWB1 the beam is focussed down to half its transverse size by means of a steep rise of B_z, which finally ends at a level of $1800\,Gauss$ and staying constant there until it decays to zero at the middle of the first accelerating section where the last solenoid ends. The longitudinal dependence of B_z and the maximum horizontal beamsize are shown in Figs. 4.4.4 and 4.4.5.

The normalized horizontal and vertical rms-emittance ϵ_n^{rms} as a function of the position z along the injector is plotted in Fig. 4.4.6. Starting with $1.8\,\pi\,mm\,mrad$ at the gun exit as calculated with EGUN the normalized rms-emittance $60\,cm$ further downstream was measured to be about $3\,\pi\,mm\,mrad$ for a $7\,nC$gunpulse $(2\,ns\,/\,3.5\,A)$ by means of the pepperpot technique [10]. Nevertheless this value is heavily deteriorated when entering TWB1 and stays almost constant at around $100\,\pi\,mm\,mrad$ after that. Off axis particles suffer from transverse forces in the electromagnetic field of TWB1. As they vary in time with the S-band frequency each longitudinal segment of the bunch is affected in a different way, which leads to a so called RF-induced emittance growth. With 200° of S-band the bunch is quite long when entering TWB1. Therefore this effect is most severe in the first few cells of it. When the bunch is short all particles are more or less affected in the same manner and the emittance stays constant. This effect can be reduced by decreasing the transverse or longitudinal beamsize or both. Since compression transversely or longitudinally is easier with a reduced bunchcharge the emittance growth will profit from the SBLC parameters.

Conclusion A feasible concept for the injector linac complex of the SBLC was presented. The SBTF scheme of bunchtrain production and bunch compression, which has been partially commissioned, can be copied for a SBLC injector, when replacing the first subharmonic buncher by a 166 MHz system. Since no switching between different interbunch spacings and a much smaller bunchcharge is required, the SBLC parameters will be easier to achieve compared with the SBTF layout. Acceleration up to the damping ring energy will be done adopting the same technique as proposed for the SBLC main linac.

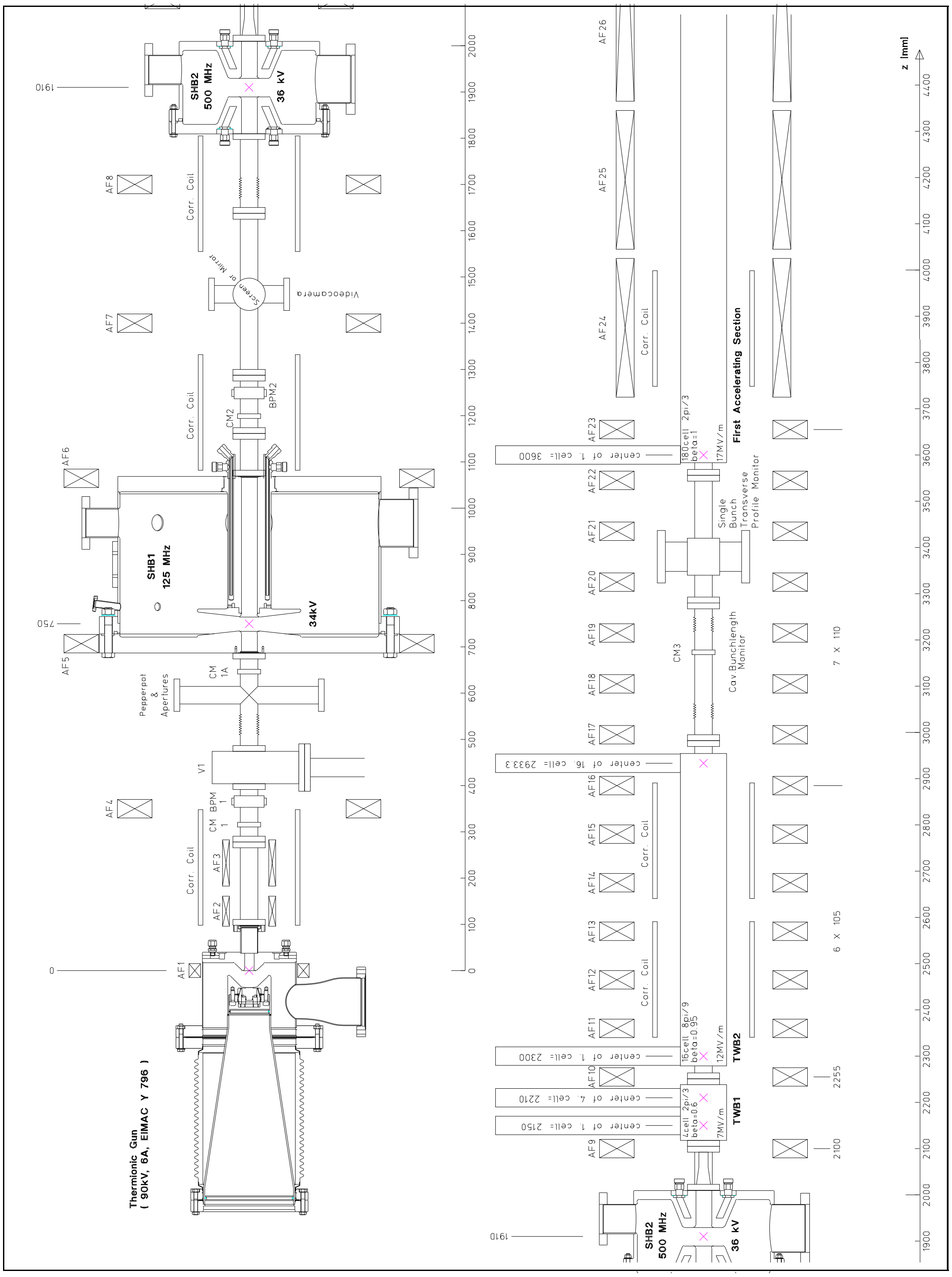

Figure 4.4.1: *Layout of the injector for the SBTF.*

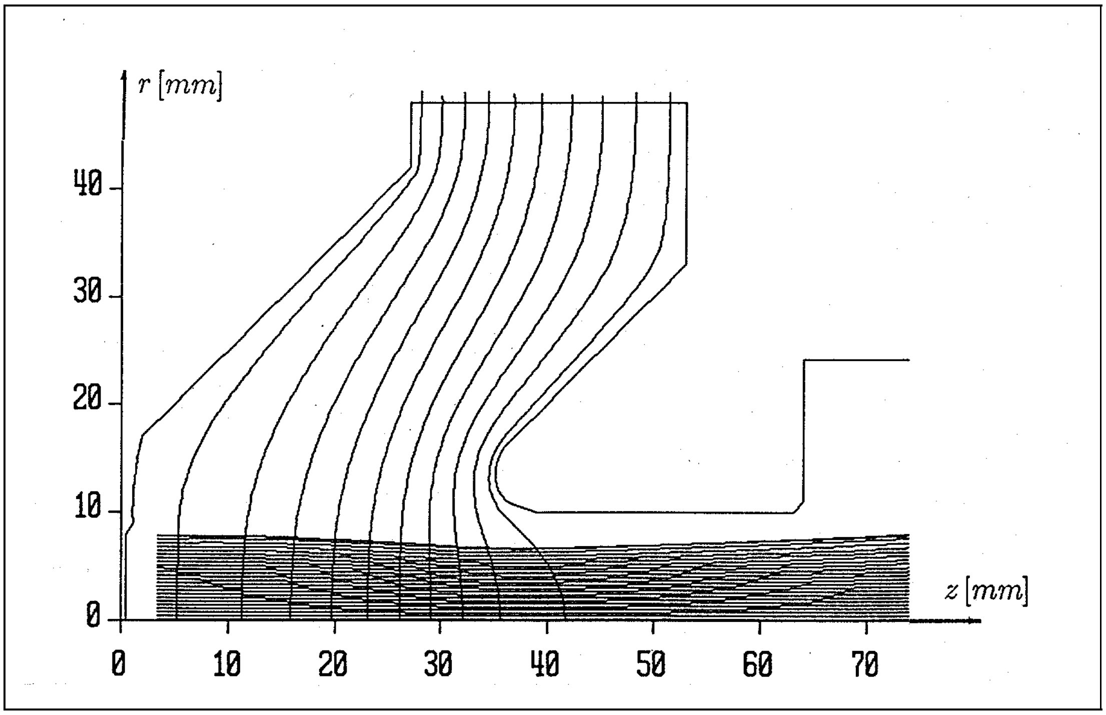

Figure 4.4.2: *Gun geometry with equipotential lines and space charge limited electron rays calculated at* $90\,kV$.

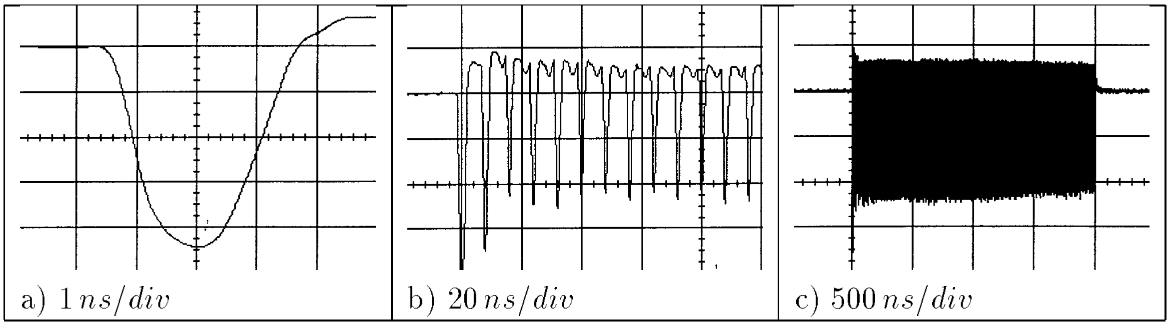

Figure 4.4.3: *Measured gunpulses at CM1. The first pulse of the bunchtrain a), the initial part b) and the whole bunchtrain c) of 250 bunches with* $8\,ns$ *spacing.*

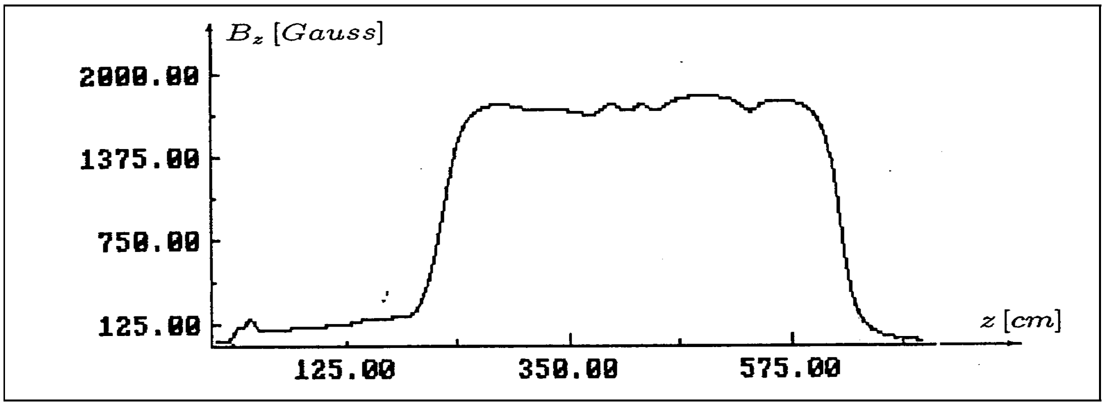

Figure 4.4.4: *Solenoidal fieldstrength B_z along the injector.*

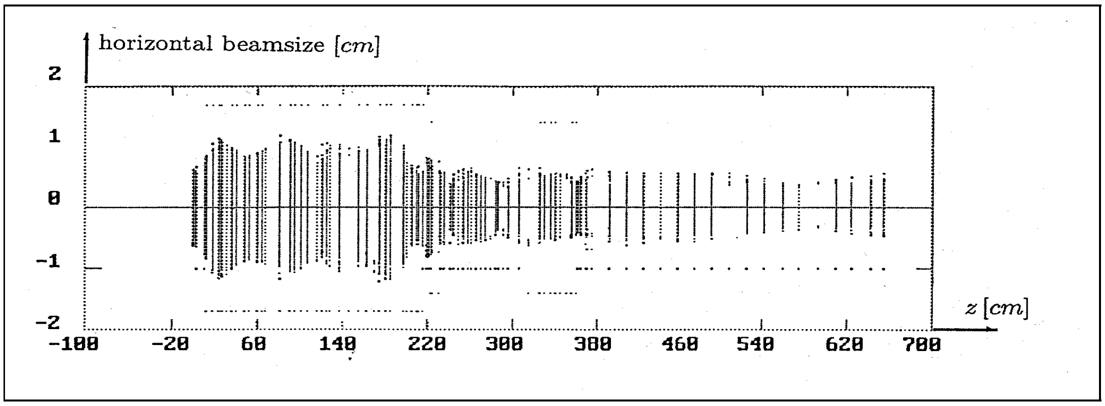

Figure 4.4.5: *Maximum horizontal beamsize and given aperture along the injector.*

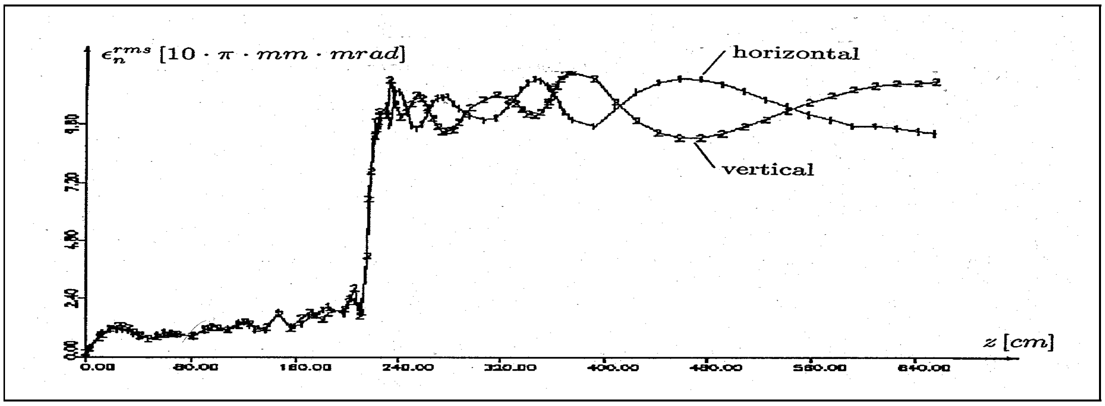

Figure 4.4.6: *Normalized horizontal and vertical rms-emittance along the injector.*

4.4.2 Positron Source

4.4.2.1 Introduction

A fundamental intensity limit for positron sources is given by the thermal stress which is built up in the conversion target due to the energy deposition of the primary beam. In case of the SBLC a complete bunch train contributes to the thermal stress in the target. Between successive linac pulses the target can be rotated so that the heat load is distributed over the target and contributes only to the average heat load. In Table 4.4.2 the design parameters of SBLC are compared with parameters reached at the SLC positron source which is the positron source with the highest intensity operating so far.

The SLC source is operating close to the stress limit of the target. An extension of this kind of source by 2 orders of magnitude in intensity seems to be impossible with a reasonable effort of technological development. Therefore a new concept based on the conversion of high energy wiggler radiation in a thin target has been developed [11, 12]. The scheme allows also to produce polarized positrons but the technological demands for a polarized source are higher than for an unpolarized source. The present design is for an unpolarized source but allows for a later upgrade to produce polarized positrons.

parameter	SLC	SBLC
# of positrons p. pulse	$3...5 \cdot 10^{10}$	$3.66 \cdot 10^{12}$
# of bunches p. pulse	1	333
pulse duration	3 ps	2 μs
bunch spacing	8.3 ms	6 ns
repetition frequency	120 Hz	50 Hz

Table 4.4.2: *Comparison between SBLC and SLC parameters.*

4.4.2.2 General Layout

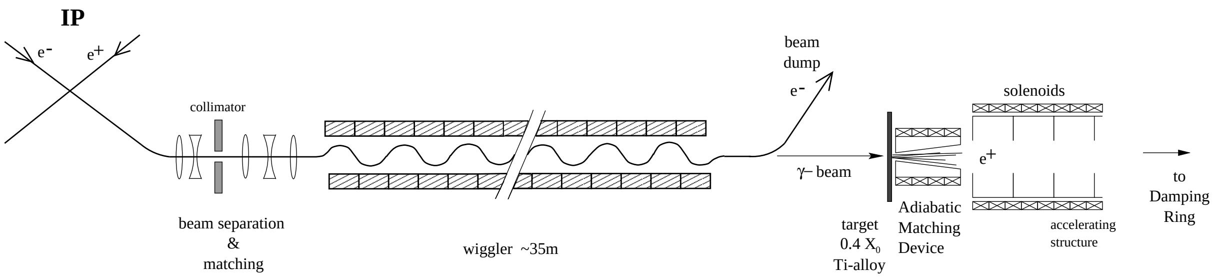

Figure 4.4.7: *Sketch of the positron source layout.*

A schematic layout of the source is shown in fig. 4.4.7. The source is designed to produce twice as much positrons as required. The 250 GeV electron beam is used after collision as primary beam for the positron production. Due to the strong beam-beam forces during the interaction process the emittance of the beam is increased and the energy distribution has developed a long tail of low energy particles. The outgoing electron beam is separated from the incoming positron beam and then collimated in order to remove the low-energy tail. More than 80% of the particles pass through the optics (see section 4.4.2.3). The final beam emittance is $\epsilon_x < 1 \cdot 10^{-8}$ m and $\epsilon_y < 1 \cdot 10^{-9}$ m, sufficiently small to match the beam to the successive wiggler section. The wiggler is a conventional wiggler of 35 m length. Here photons are generated with a broad energy distribution extending up to above 70 MeV. A dipole section of $\approx$30 m length separates the electron beam from the photon beam and guides it to the beam dump. The photons are used to produce electron-positron pairs in the thin conversion target. A minimum spot size of the photon beam on the target of σ_{min}=0.5mm can be realized. The heating of the target is dominated by the ionization losses of electrons and positrons given by $E_{dep} \approx 2$ MeV cm^2/g per charged particle. Thus the temperature rise of the target ΔT can be estimated as:

$$\Delta T[K] = \frac{2Ne \cdot 2 \cdot 10^6}{c \cdot A \cdot \eta} \tag{4.4.1}$$

where c denotes the heat capacity in Jg^{-1}K^{-1}, A the source area in cm^2 and η the efficiency of positron capture after the target.

In order to get N positrons, $2N/\eta$ particles (electrons and positrons) have to emerge from the target. The heat load of the target is determined by three more or less free parameters:
- the heat capacity of the target material c,
- the efficiency of the capture optics η,
- the source area A.

An increased source area counteracts a high capture efficiency, because the phase-space density of the emerging positrons is reduced, thus a small source area is favorable. Since in the present design the photons are generated in a wiggler, rather than by bremsstrahlung in the target, a high positron yield is reached with a thin target of only 0.4 radiation length (X_0) thickness. Compared to a conventional source the thermal stress of the target can be significantly reduced by two effects:
- one is able to use a material with low nuclear charge Z which in general have a high heat capacity.
- the divergence of the positron beam is small due to the reduced scattering in the target and hence the capture efficiency is increased. A conventional target requires many radiation lengths for the full development of the electromagnetic cascade. Positrons which are produced in the first steps of the cascade will not emerge from the target due to the ionization losses inside the material. The ionization loss per radiation length depends on the material and is lower for high Z materials. Hence a high Z material has to be used in a conventional source in order to reach a high positron yield. In thin targets, however, the conversion efficiency is in first order independent of the

material, hence it is possible to use a low Z material which has a higher heat capacity (Dulong-Petit-rule). In the present design a Titanium alloy is foreseen as conversion target which allows to increase the particle density in the target by about an order of magnitude as compared to a high-Z Tungsten-Rhenium alloy.

The second advantage of a thin target is the reduced multiple scattering which determines the transverse beam emittance of the positrons. The rms scattering angle scales with the square root of the path length of the particle in units of X_0. The rms scattering angle scales non-linearly with the target thickness since in a conventional source most of the positrons are produced close to the target exit. Nevertheless, the transverse momenta of the positrons produced in a thin target are considerably smaller than the transverse momenta of positrons from a conventional source. Therefore the capture efficiency is increased by a factor 4-5 in the present design as compared to a conventional source.

The capture optics behind the target is of a conventional design. Since the positrons have a broad distribution of transverse and longitudinal momenta they have to be accelerated in a acceleration section embedded in a solenoid field. The acceptance of a solenoid channel is characterized by a large spot size and small angles while the positrons emerging from the target have a small spot size and large angles. To match the positrons to the acceptance of the solenoid, an Adiabatic Matching Device (AMD) is used. It consists of a tapered solenoid field which starts with a high initial field and tapers down adiabatically to the constant end field.

After acceleration to an energy of 150-200 MeV the positrons are separated from the electrons and the photons in a magnetic chicane. The electron and the photon beams are dumped and the positron beam is accelerated to its final energy and transferred to the damping ring.

The safety margin of a factor of two in the positron production rate is valid for 250 GeV electron beam energy. For operation at lower energy this margin is reduced. Without modifications, the source can be used down to about 160 GeV. Operation at lower energy with full design positron beam intensity requires to increase the length of the wiggler.

In the following the components of the positron source will be discussed in more detail.

4.4.2.3 Spent Beam Capture System

Due to the very strong beam-beam force the particles which do not pass through the center of the opposing bunch are strongly deflected. This disruption effect causes a broadening of the angular distribution after the interaction. The beam size remains nearly constant or even decreases due to the focusing pinch effect.

For all investigations a data set of roughly 12,000 particles was created with a beam-beam simulation code using the parameters at the interaction point. Fig.4.4.8 shows the phase space distributions both in the horizontal and vertical plane. The differences in the distribution are caused by the flatness of the beam.

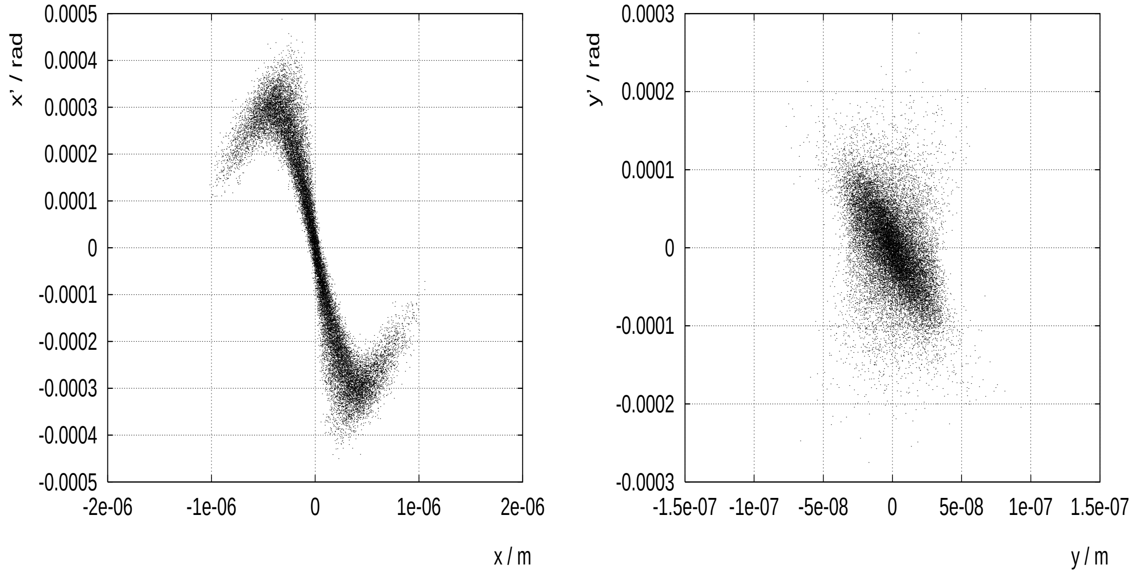

Figure 4.4.8: *Horizontal and vertical phase space distribution after the interaction.*

The deflected particles emit high-energy synchrotron radiation (beamstrahlung). This statistical process causes a broad energy spread of the disrupted beam and a mean energy loss of 3% of the initial energy. A non negligible part of the beam has lost more than 10% energy. Fig.4.4.9 shows the energy distribution after the interaction.

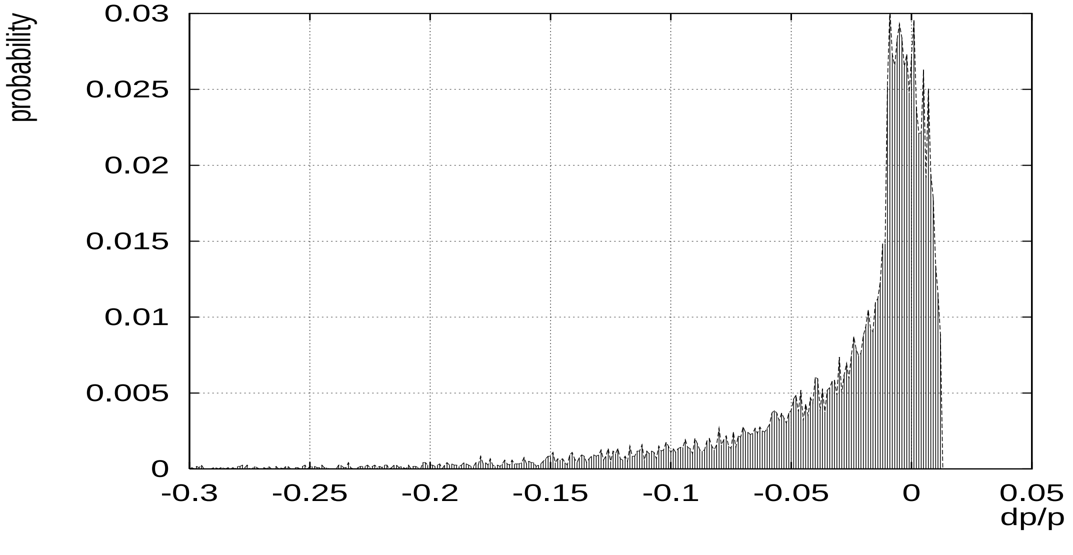

Figure 4.4.9: *Energy spectrum of the disrupted beam*

The disrupted electron beam leaving the IR is separated from the incoming positron beam by a using a crossing angle of 6 mrad. Therefore the disrupted beam after the IR

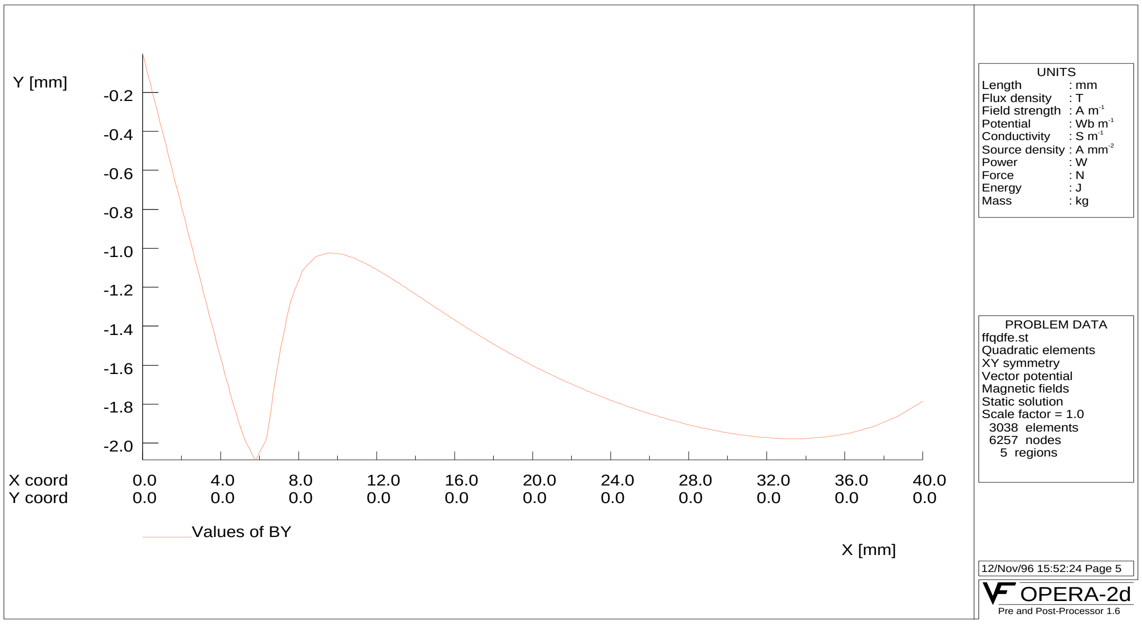

Figure 4.4.10: *Vertical magnetic field as a function of distance from axis. The spent electron beam enters the quadrupole with a horizontal offset of 13 mm.*

enters the final doublet (FD) for the incoming positron beam 13 mm displaced from the magnet axis. The field of the final quadrupole with a geometry as shown in Fig.4.7.16 in section 4.7 has been analyzed numerically. Fig.4.4.10 shows the vertical magnetic field as a function of distance to the symmetry axis of the quadrupole. The shape shows that there are higher order multipole components which are changing along the path through the FD due to the increasing distance from the axis. The emittance growth caused by the non-linearity of the field and by the synchrotron radiation has been determined by particle tracking simulations. It is found that the horizontal emittance is about two orders of magnitude larger than that of the incoming beam.

For the investigation of the beam capture optics the matched optical functions after the FD are determined for sub-ensembles of the spent beam obtained by applying an energy cut removing part of the beam which has lost more than a certain fraction of energy.

At the end of the FD the separation from the incoming positron beam is 4.2cm with a total angle of 8.05mrad (2.05mrad due to the deflecting effect of the FD field). This allows to place a doublet of half-quadrupoles 10 m downstream from the FD. A bending magnet and a second quadrupole doublet are used to match the optical functions to the beginning of the chromatic correction section.

Chromatic Correction System

After initial separation of the spent beam as described above a magnet lattice basically very similar to the horizontal CCS for the incoming beam follows. The boundary conditions for the design of this beam-optical system are:

- The geometry of the beamline should be such that it fits together with the FFS into the same tunnel.
- The bending magnets have to be sufficiently weak to avoid strong emittance growth from synchrotron radiation.
- The momentum bandwidth has to be large to accomodate a large fraction of the broad momentum distribution of the spent beam.

Starting from a basic layout which fulfills the first two conditions an optimization of the bandwidth is performed by adding sextupoles at strategic positions in the lattice. An ensemble of trajectories representative of the spent beam properties is tracked through the system and optimum sextupole strengths which lead to a minimum beam emittance at the end of the lattice are determined. The procedure is similar to the one applied in ref. [13]. The amount of spent beam accepted by the system is directly related to the maximum tolerable emittance in the wiggler. As shown in fig. 4.4.12, the horizontal emittance starts growing rapidly if more than 85...90% of the beam is passed through the beamline, indicating that the low-energy tail falls outside the bandwidth of the optics. In this range the vertical emittance does not exceed the value of $\varepsilon_y = 10^{-9}$ m which is five times lower than required for the unpolarized source. So due to the limitations on the horizontal emittance, even with an optimized achromatic system it is not possible to transport the whole beam from the IR on through the capture optics and afterwards through the wiggler. Thus the low energy tail which contains a considerable fraction of the beam power has to be collimated.

After the end of the CCS's the optics is continued with a drift space of 20 m and a quadrupole triplet. The beam is focused such that the radiation emitted in a 35m long wiggler hits the target in a focal point 30 m behind the wiggler i.e. 70 m behind the last quadrupole doublet.

Fig. 4.4.13 shows the geometry of the whole capture system with the wiggler and the drift space to the target with regard to the beam delivery system of the oncoming positron beam. The separation between the two beamlines is sufficiently small to fit into a tunnel of 4 m diameter.

The optimization of the optics and the need to collimate the major part of the low energy particles in regions without optical elements (see Table 4.4.3) results in a capture efficiency of 87.5% of the disrupted electron beam.

Fig. 4.4.14 and fig.4.4.15 shows the maximum beam envelopes of the disrupted beam along the capture optics with the position of the collimators. The 35 m long wiggler is positioned between 450 m and 485 m downstream from the IP. In this region the maximum vertical beam size does not exceed values of 2 mm.

Inside the wiggler in the horizontal plane some particle amplitudes are growing although the whole beam is focused on the target. The reason is the remaining chromaticity which causes a defocused low energy subset of the captured beam.

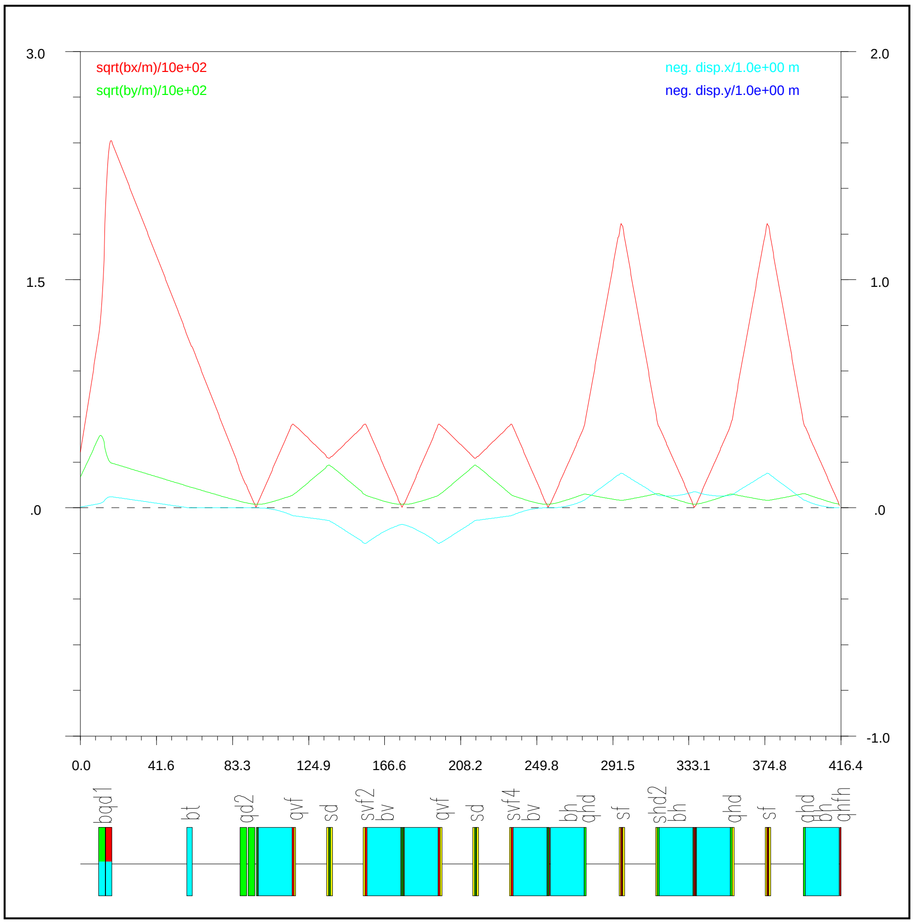

Figure 4.4.11: *Optics of the spent beam capture system from the end of the FFQ's to the end of the CCS.*

Stability of the positron source

The efficiency of the capture optics for the disrupted electron beam depends on the parameters of the interacting bunches. The optics and the collimation system described above are developed for interacting bunches with design parameters. In reality, the capture efficiency for the disrupted beam may not be constant but depends on the energy spread due to beamstrahlung. As explained above, the beamstrahlung is a function of the bunch charge and other interaction parameters.

If we consider a perturbation of the interaction, for example a displacement of the orbit, the spent electron beam would not be disrupted like in a head-on interaction. Hence the number of captured electrons passing the collimation system can be higher. The positron bunches in the next pulse have a higher charge which in turn causes a higher electron beam energy spread after the IP. The fixed energy acceptance of the capture optics then leads to a lower intensity electron beam for the photon production. In the second pulse after the perturbation the positron bunch has a lower charge and so the system can oscillate. For a stable operation of the linac, this oscillation must be

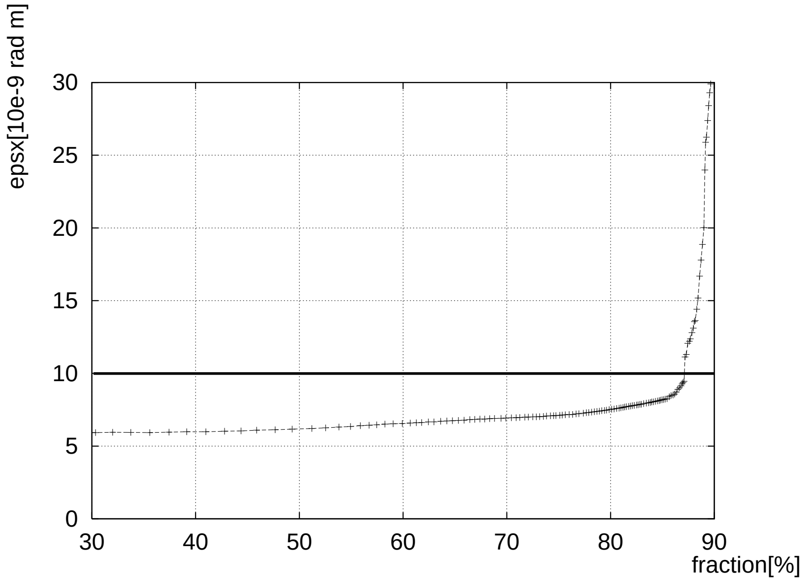

Figure 4.4.12: *Horizontal emittance at the end of the CCS vs. percentage of the initial beam obtained by an energy dependent cut. The thick line shows the horizontal emittance limit for the unpolarized source.*

Collimator	Distance from IR doublet [m]	Collimated power [KW]	Remarks
COL0	0.00-10.00	67.57	between the IR doublet and the 1st half-quad
COL1	38.23-58.23	70.08	between the 2nd half-quad and the first dipole
COL2	61.23-87.40	305.02	behind the first dipole and the following quad
COL3	137.90-154.90	214.56	driftspace inside the CCS
COL4	197.90-214.90	27.99	driftspace inside the CCS
COL5	217.90-234.90	128.50	drfitspace inside the CCS
COL6	377.90-394.90	75.37	driftspace inside the CCS
COL7	416.40-436.40	41.63	driftspace after the CCS
COL8	445.40-450.40	8.17	5m before the wiggler

Table 4.4.3: *Collimator positions and collimated beam power.*

damped.

The investigation of stability is started considereing the maximum possible perturbation, i.e. the case that the bunches do not interact at all. The electrons pass the collimation system completely and the positron bunches for the next pulse have a 14% higher charge than designed. The next interaction is simulated with this asymmetric bunch charges. The outgoing disrupted electron beam was tracked through the capture optics to obtain the efficiency for the following pulse. This yields a new (reduced)

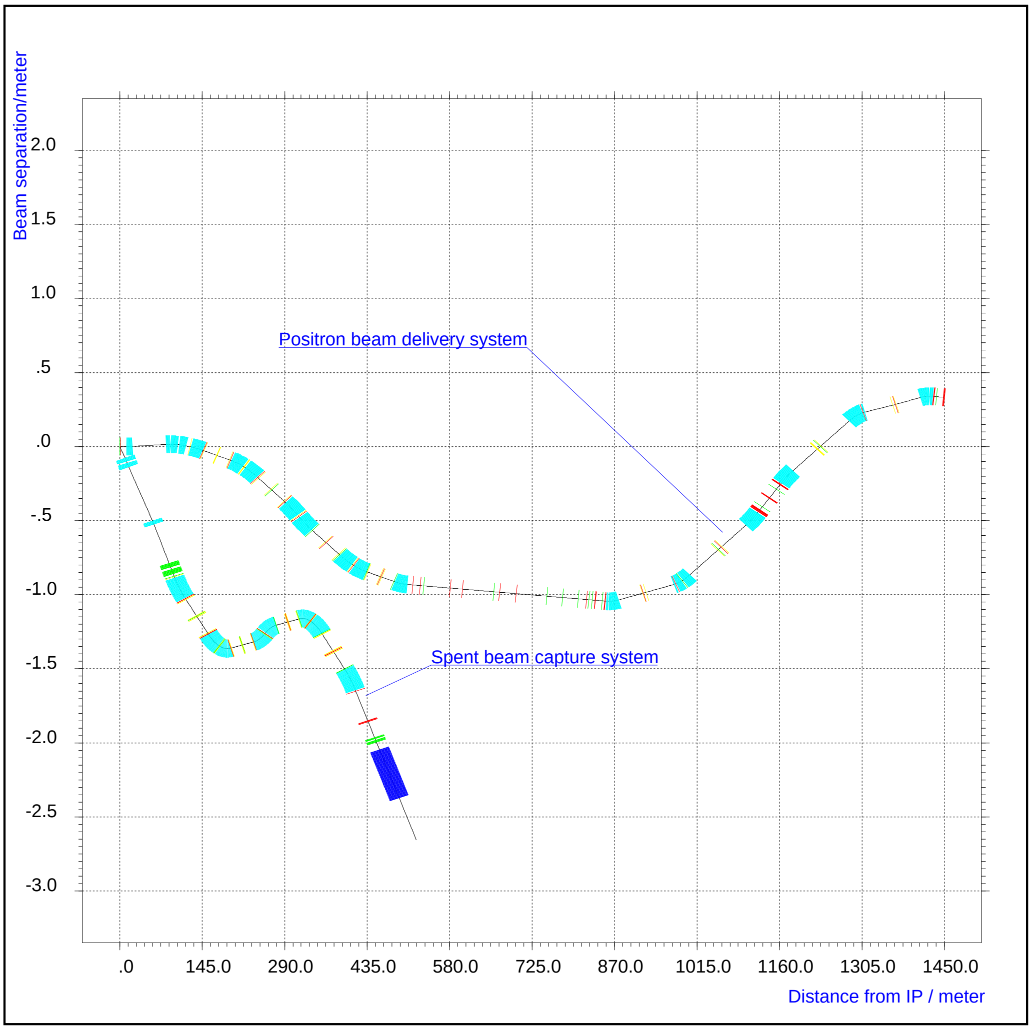

Figure 4.4.13: *Beam line for the disrupted beam with the 35 m long wiggler (lower branch) and the incoming positron beam (upper branch). At the end of the capture optics the separation is 1.7 m.*

positron intensity for the next interaction, etc. Fig. 4.4.16 shows the resulting behavior of the bunch charge as a function of interactions after the perturbation. The oscillation decreases and so the positron source can be operated stably from this point of view.

Efficiency Gain due to Parameter Change at the IP

The efficiency of the capture system is limited by higher order geometric and chromo-geometric aberrations. With a relatively moderate adjustment of the interaction parameters, both the horizontal beam emittance and the energy spread can be reduced, thus decreasing the population of the tails in the spent beam which have to be collimated. This is demonstrated in Fig. 4.4.17 where the spent beam capture efficiency is

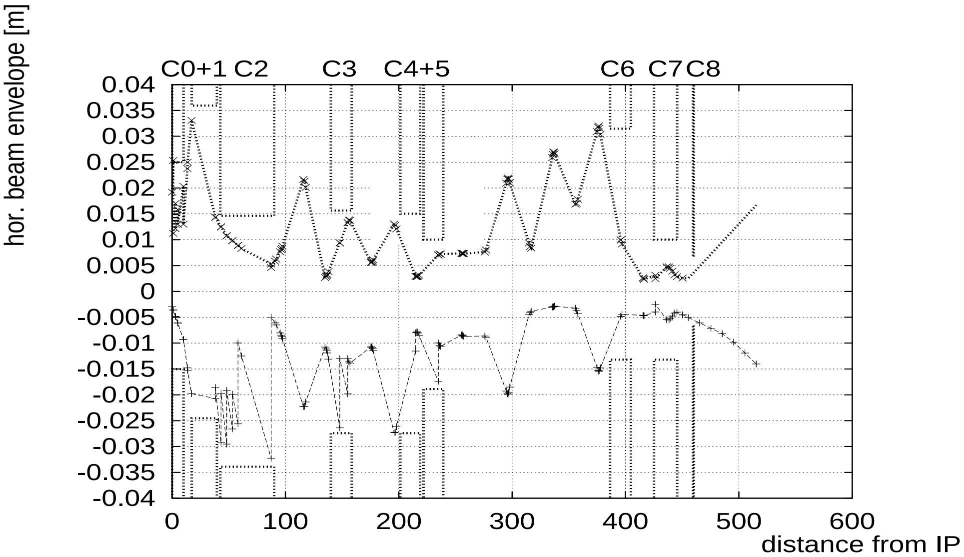

Figure 4.4.14: *Horizontal envelope for an ensemble containing 87.5% of the spent beam.*

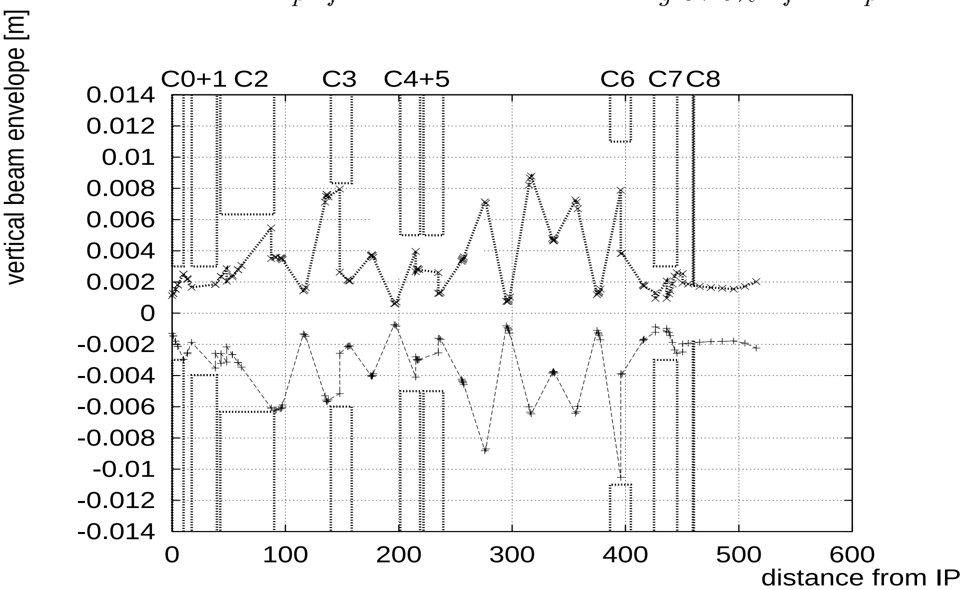

Figure 4.4.15: *Vertical envelope for an ensemble containing 87.5% of the spent beam.*

shown as a function of the horizontal beta of the positron beam at the IP. An increase of $\beta_x^*(e^+)$ by a factor of two already reduces the amount of collimated spent beam from 12.5% to 4%. At the same time, the luminosity is reduced by only about 20%, which can be compensated by a slight reduction of the vertical beam emittance. With such a parameter modification, an efficient operation of a polarized positron source would be greatly facilitated.

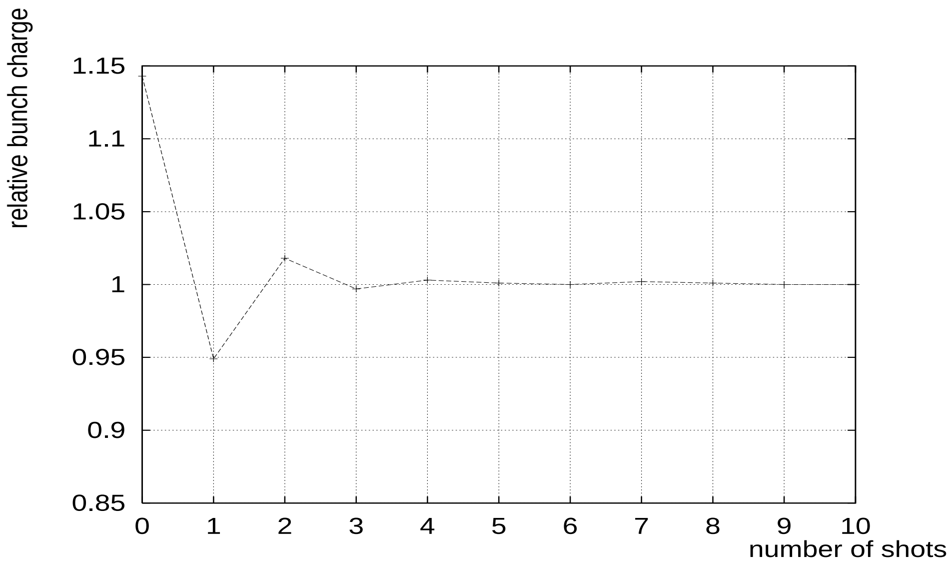

Figure 4.4.16: *Oscillations of the positron bunch intensity after one missing interaction. The bunch charge reaches the design value after 4 pulses.*

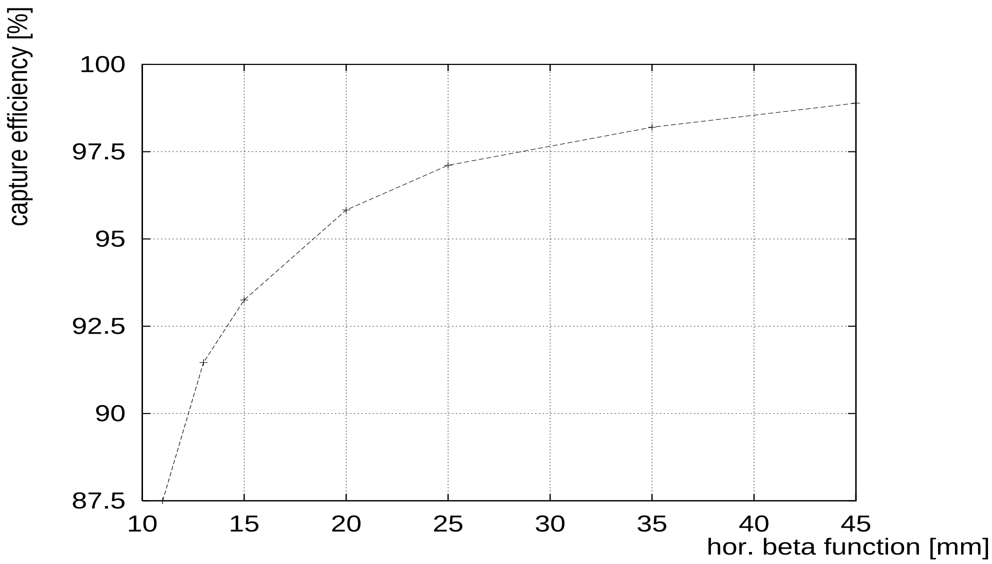

Figure 4.4.17: *Capture efficiency as a function of the horizontal β-function of the positron beam at the IP. Starting from the design value of 11 mm the capture efficiency reaches 98.9 % of the disrupted beam for $\beta_x^*(e^+) = 45\,mm$.*

4.4.2.4 Wiggler

A planar wiggler consists of a row of short dipole magnets with constant field strength but alternating field direction. For a large period length λ_w the photon number spectrum can be approximated by the well known photon number spectrum of dipole magnet. Fig. 4.4.18 shows the photon number spectrum of a 1m long dipole with a magnetic field of B=1.7 T.

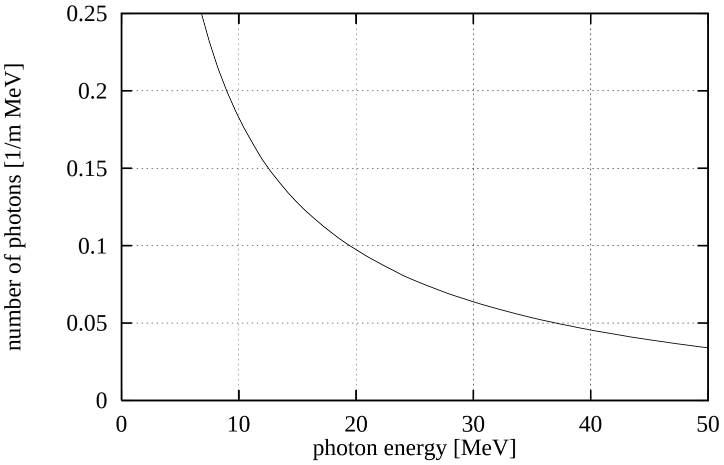

Figure 4.4.18: *Photon number spectrum of a planar wiggler with B=1.7 T at a beam energy of 250 GeV.*

In order to reach a small spot size of the radiation on the target the electron beam is focused through the wiggler onto the target. The contribution of the natural opening of the wiggler radiation to the spot size can be approximated by:

$$\sigma_{SR} \approx \frac{eB\lambda_w}{2\pi p_e} \cdot (L/2 + D) \tag{4.4.2}$$

Here p_e denotes the electron momentum, L the wiggler length and D the driftspace between the wiggler and the target.

For $L \approx$35 m and $D \approx$30 m the period length λ_w should not exceed 3.2 cm in order to reach a spot size contribution of 0.5 mm. Since the electron beam emittance is quite small a gap height of only 5mm is sufficient to transport the beam through the wiggler. Today wigglers and undulators based on permanent magnet technology are widely used in both synchrotron radiation sources and free electron lasers. Period length and magnetic fields similar to the values discussed above are not unusual for these devices. In contrast to the sinusoidal field distribution of a synchrotron radiation device a more rectangular distribution would be favorable for the positron source in order to keep the length of the wiggler shorter. Various inexpensive proposals of wigglers with a rectangular field distribution and similar period length are discussed in ref. [14].

4.4.2.5 Target

A high energy photon passing through a material can create an electron positron pair in the field of a nucleus (pair production). These charged particles again lose energy on their way through the material via collisions with electrons (ionization) and radiation processes in the field of a nucleus (bremsstrahlung). The ionization losses account for the majority of heat deposition in the material, while photons produced via bremsstrahlung may once more produce electron positron pairs. This sequence continues, i.e. the number of electrons, positrons and photons increases exponentially, while the mean energy of the particles decreases. The development of the shower decays when the particle energy drops below $\approx$10 MeV because the energy loss due to ionization exceeds the production of photons at low energies. Bremsstrahlung and pair production are essentially inverse processes, hence they can be characterized by a common parameter called the radiation length X_0. The radiation length of a material is approximated by:

$$X_0^{-1} = \frac{4\alpha r_e^2 N_A \rho}{A} \cdot Z(Z+1) ln(183 Z^{1/3}) \qquad (4.4.3)$$

where A is the atomic weight, Z the nuclear charge, ρ the density of the material and N_A Avogadro's number.

Since for important electromagnetic processes (bremsstrahlung, pair production, multiple scattering) some or all of the dependence upon the medium is contained in the radiation length, it is convenient to measure the target thickness in terms of the radiation length. Besides bremsstrahlung and pair production the shower development is influenced by many other processes like Compton scattering, Møller scattering, Bhabha scattering, photo effect etc. A complete treatment of the development of an electromagnetic cascade is possible only with a numerical simulation code. The following calculations have been performed with the code EGS4 [15]. The EGS code is a general purpose package for the Monte-Carlo simulation of electromagnetic showers. Since its formal introduction in 1978 it has been extended and improved and a lot of comparisons with experiments have verified the performance.

Fig. 4.4.19 shows the positron yield per electron as function of the target thickness for different materials. The incoming photon beam has been generated in a 1m long wiggler of 1.7 T magnetic field. For a target thickness above $0.5\,X_0$ the yield increases slowly before it starts to decrease again. Since the multiple scattering increases the beam emittance with increasing target thickness, the optimum overall efficiency, i.e. including the capture efficiency, is found at about $0.4\,X_0$. At this thickness the yield for a low Z material like Titanium is only about 16 % lower than for Tungsten.

In Fig. 4.4.20 the temperature distribution in a Titanium target induced by a single train of wiggler photons from a 35 m long wiggler of 1.7 T is shown. As a safety margin the number of positrons produced in this simulation exceeds the nominal value behind the capture optics by a factor of two.

The maximum temperature rise of 760 °C is slightly higher than the maximum temperature reached in a Tungsten-Rhenium target close to the stress limit given in ref. [16]. The density of charged particles is about 5 times higher in the Titanium

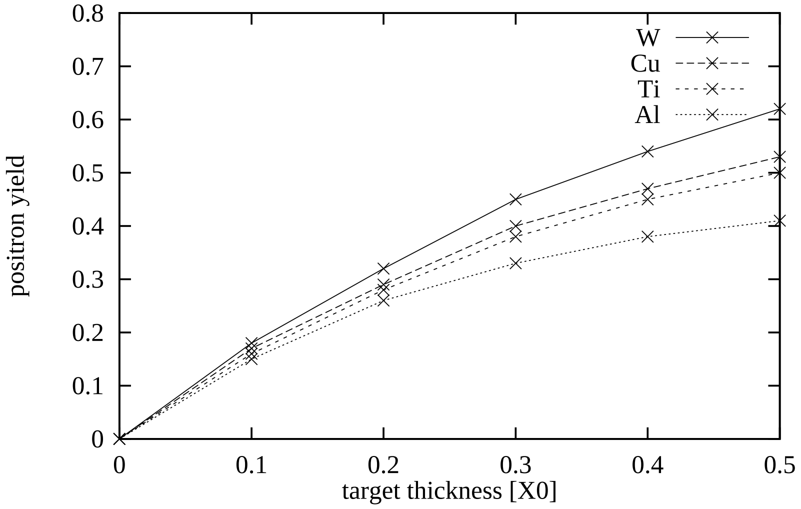

Figure 4.4.19: *Positron yield vs. target thickness for different materials. The photons are generated by a 250 GeV electron beam in a 1 m long wiggler of 1.7 T magnetic field.*

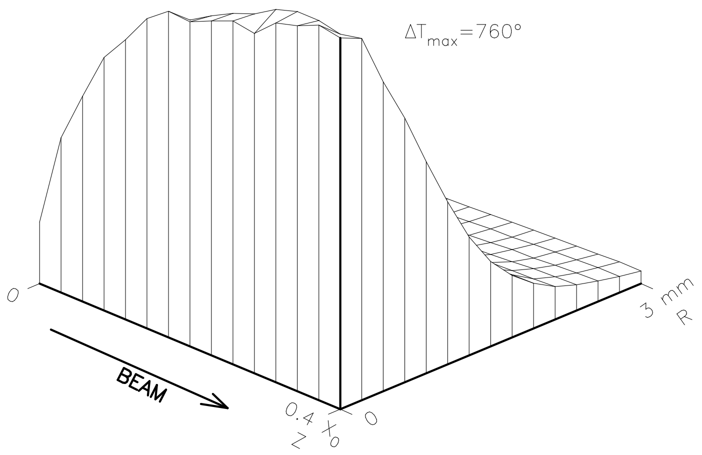

Figure 4.4.20: *Radial and longitudinal temperature distribution in the Titanium target. The spotsize of the incoming beam is $\sigma_{x,y}$=0.7 mm.*

target but due to the 5 times higher heat capacity the temperature does not increase dramatically.

Besides the temperature rise the mechanical constants of the target material have to be taken into account. Experimental data for the maximum heat load of a low Z positron conversion target are not available even though the material is used in high power collimators. In order to scale the results obtained for high Z targets to

material	c [J/kg]	α $10^{-6}K^{-1}$	E $10^{11}N/m^2$	$P_{0.2}$ $10^7N/m^2$	ΔT_{crit} K^{-1}	x_0 cm	ρ g cm^{-3}
W-26Re	0.13	5.0	4.00	91.0	455	0.35	19.3
Ti	0.52	8.4	1.16	55.0	564	3.56	4.54
Ti-5Al-2.5Sn	0.52	9.3	1.17	86.3	793	3.5	4.46
Ti-13V-11Cr-3Al	0.62	8.8	0.98	96.1	1114	3.5	4.82

Table 4.4.4: *Material constant of Tungsten-Rhenium and various Titanium alloys.*

the case of low Z targets the material constants can be combined with respect to their proportionality to the mechanical stress $P_t \approx \Delta T \alpha E$ induced by heating (α: expansion coefficient, E: elastic modulus).

The induced stress has to remain below the 0.2% yield strength $P_{0.2}$ which is the stress where the deformation of a material ceases to be elastic, $P_t < P_{0.2}$.

Table 4.4.4 lists material constants for the Tungsten-Rhenium alloy used in the SLC positron source and various Titanium alloys. The geometrical dimensions of the SLC target (thickness: 2.1 cm) and a Titanium target (thickness: 1.4 cm) as well as the dimensions of the electron and photon beam spot size on the target are comparable. Therefore the temperature distribution in the targets is similar and the ratio $P_{0.2}/\alpha E = \Delta T_{crit}$ can be used to compare the maximum temperature rise that the target can withstand. It is seen from Table 4.4.4 that the maximum temperature in a Titanium target can be up to twice as large as in a Tungsten target.

The average heat load of the target amounts to 6 kW, therefore water cooling of the target is necessary. In order to avoid a rotating feed through for the cooling water a winch mechanism can be utilized as at the SLC source [17].

4.4.2.6 Capture Optics

The particles which emerge from the target have to be accelerated in a cavity embedded in a solenoid field for focusing. Here the final emittance and the efficiency of the positron source are defined. Since, compared to the thick target of the conventional source the multiple-scattering is reduced in a thin target, the transverse momenta of the positrons emerging from the target are smaller. Fig. 4.4.21 compares transverse momenta of a SLC-like source with those of a thin target source driven by photons from a wiggler.

The smaller transverse momenta lead to a higher capture efficiency of the positrons behind the target. In order to match the emittance of the positron beam, characterized by a small spot size and a large divergence, to the acceptance of the solenoid which is determined by a large spot size and a small divergence a matching section is introduced between the converter target and the first accelerating cavity. The matching section consists of a so-called Adiabatic Matching Device (AMD), a tapered solenoid starting with a high initial field and tapered adiabatically down to the constant end field. The acceptance of the system is matched to the acceptance of the damping ring so that no particle losses occur later in the damping ring. Besides the acceptance of the damping

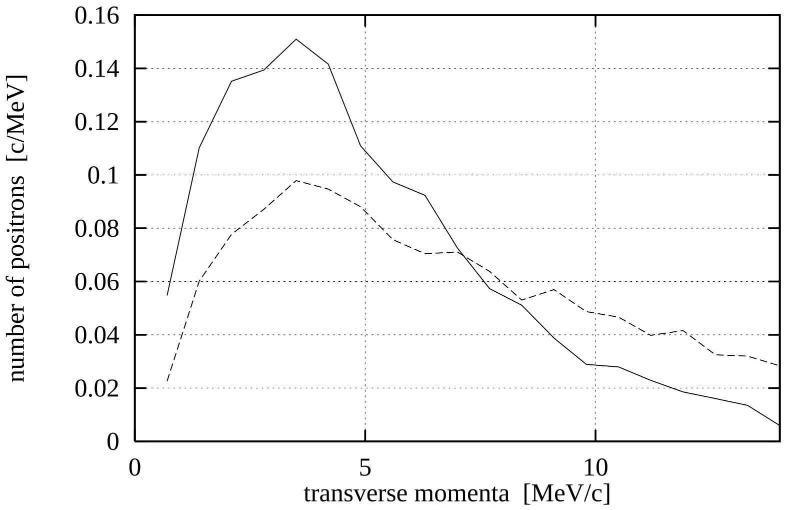

Figure 4.4.21: *Comparison of transverse momentum distribution for a SLC-like source (6X_0, W, dotted line) and a thin target as proposed here (0.4X_0, Ti, solid line).*

ring that limits the useful acceptance of the matching device two mechanisms lead to an emittance growth of the positron beam in the matching device and hence to additional particle losses:
- emittance growth due to non adiabatic fields.
- bunch lengthening due to path length and velocity differences.

R. Helm has found a solution for the particle motion in an adiabatically varying solenoid field [18] from which he derived the optimum on-axis field distribution for the matching device along the longitudinal coordinate z as:

$$B(z) = \frac{B_i}{1 + g \cdot z} \tag{4.4.4}$$

where B_i is the initial solenoid field and g the taper parameter.

The condition for an adiabatic field variation is then given as $(gp_e)/(eB_i) \ll 1$. In order to fulfill this condition for particles with higher energy the taper parameter g has to be small. However, this means that the matching section becomes long and that the bunch lengthening becomes stronger. An optimum is reached with g=30 m^{-1} in the present design. Figure 4.4.22 shows the energy distribution of the positrons as they emerge from the target and the fraction of captured particles for the optimized optics. Figure 7 shows the longitudinal distribution of the positrons behind the AMD. While the core of the distribution represents the incoming electron beam (σ_s= 0.3mm or $\approx 1°$ RF phase) a long tail has been developed due to bunch lengthening effects. The positrons in the tail will be lost in the damping ring since the curvature of the RF leads to a large energy deviation of these particles. In the simulation an energy acceptance of $\pm1\%$ corresponding to an RF phase of $\pm7.5°$ is assumed.

A capture efficiency of 17 % is reached with an initial field of $B_i = 7$ T. Fields of up to 8 T have already been realized [19]. For the preacceleration a standard S-band structure

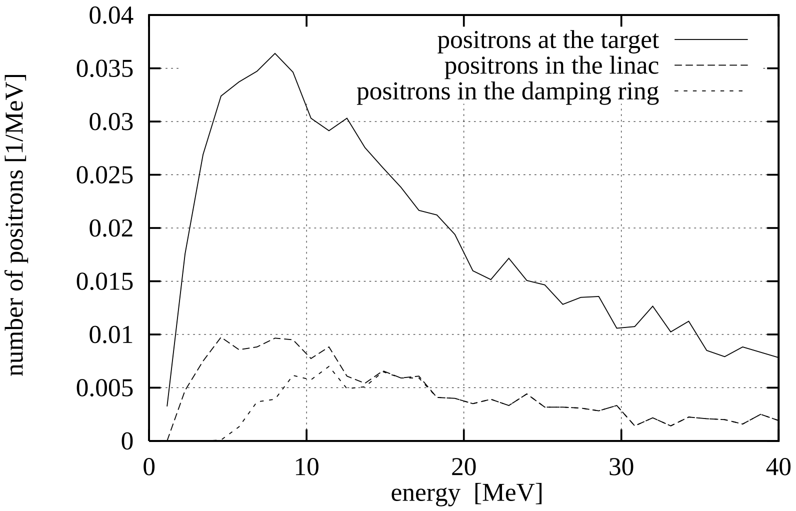

Figure 4.4.22: *Energy distribution of the positrons after the target (solid line) and the fraction of captured positrons (dashed lines).*

embedded in a solenoid field of 0.7 T can be used. With a gradient of 20 MV/m the bunch lengthening in the first acceleration section is sufficiently suppressed. Table 4.4.5 collects important parameters of the positron source.

4.4.2.7 Low Intensity Auxiliary Source

For the commissioning of the positron damping ring, the main positron linac etc., a source that works independent of the main electron linac would be desirable. Most of this work can be done or even has to be done at low intensities. Therefore a conventional low intensity source will be integrated into the high intensity source. An electron beam of only 500 MeV is sufficient to produce a few per cent of the design positron current using the thin Titanium target and the capture optics of the high intensity source. In this case the heat load of the target is high but does not reach the limits that have been previously discussed. The electron source for the low intensity positron source can also be used to provide electrons for the main linac for electron-electron and gamma-gamma collisions, respectively.

4.4.2.8 Potential Upgrade to a Polarized Positron Source

The proposed positron source allows also to produce polarized positrons as it was originally proposed by V. E. Balakin and A. A. Mickhailichenko [12, 11]. The technological demands are, however, much stronger in this case. Therefore the polarized source is regarded as a potential upgrade option.

In order to produce circularly polarized photons a short period helical undulator of about 100 m length has to be used instead of the planar wiggler. Since only the on-axis photons are completely circularly polarized off-axis photons have to be scraped

Wiggler	
peak field	1.7 T
period length	31 mm
gap height	5 mm
γ-spot size on target	0.7 mm
# of photons p. electron	368
mean photon energy	22 MeV
photon beam power	230 kW
Target	
material	Ti-alloy
thickness	1.42 cm ($0.4X_0$)
pulse temperature rise	760 K
av. power deposition	6 kW
Adiabatic Matching Device	
initial field	7 T
taper parameter	30 m^{-1}
end field	0.7 T
capture cavity iris radius	11 mm
General	
capture efficiency	17 %
# of positrons p. electron	2
norm. e^+-beam emittance	0.007 m
total energy width	$\pm$30 MeV
required D.R. acceptance	0.04 m

Table 4.4.5: *Overview of the positron source main parameters.*

off. This requires that the spot size of the photon beam on the target is dominated by the natural opening of the radiation rather than by the emittance contribution of the electron beam. Therefore the distance between the undulator and the target has to be increased to 150 m and the electron beam emittance has to be decreased to $\epsilon_x = 5 \cdot 10^{-10}$ m and $\epsilon_y = 10^{-10}$ m. The emittance requirement can easily be fulfilled for the vertical plane but is difficult to achieve in the horizontal plane. Improvements of the interaction region layout are necessary to avoid the strong emittance growth resulting from the offset of the outgoing beam in the final quadrupole.

The parameters of the helical undulator are demanding and have not been reached so far. With a period length of 1 cm an on-axis field of 1.3 T has to be reached. These parameters can be realized only with superconducting technology at a gap radius of only 2 mm. A detailed technological design of an undulator with the required parameters has not been worked out yet.

The polarization of the circularly polarized photons is transferred to the electron-positron pairs during pair production. For the calculation of the processes in the target the EGS4 code has been extended. The code includes polarization effects for pair production, Bremsstrahlung and Compton scattering and yield a maximum longitudinal polarization of a polarized positron source of 50-60%.

Bibliography

[1] R. Alley et al., *The Stanford Linear Accelerator Polarized Electron Source*, Nucl. Instrum. And Meth. A365 (1995) 1.

[2] M. Woods et al., J. Appl. Phys. 73 (1993) 8531.

[3] A. Herrera-Gómez and W.E. Spicer, Proc. SPIE 2022 (1993) 51.

[4] D. Schultz et al., *The Polarized Electron Source of the Stanford Linear Accelerator Center*, SLAC-PUB-6606, August 1994; presented at 17th International Linear Accelerator Conference (LINAC 94), Tsukuba, Japan, 21-26 Aug 1994.

[5] H. Tang et al., *Experimental Studies of the Charge Limit Phenomenon in NEA GaAs Photocathodes*, SLAC-PUB-6515, June 1994; presented at 4th European Particle Accelerator Conference (EPAC 94), London, England, 27 Jun - 1 Jul 1994.

[6] K. Aulenbacher et al., *RF Guns and the Production of Polarized Electrons*, CLIC Note 303 and NLC-Note 20, May 1996.

[7] J.E. Clendenin, *Polarized Electron Sources*, SLAC-PUB-95-6842, May 1995; Talk given at 16th IEEE Particle Accelerator Conference (PAC 95) and International Conference on High Energy Accelerators, Dallas, Texas, 1-5 May 1995.

[8] M. Schmitz, D. Yeremian, *The Injector for the S-Band Test Facility at DESY*, Proceedings of the 1994 International Linac Conference p.71-73, Tsukuba, Japan.

[9] M. Schmitz et al., *First Tests at the Injector for the S-Band Test Facility at DESY*, Proceedings of the 1995 Particle Accelerator Conference p.929-931, Dallas, Texas, USA.

[10] M. Schmitz, *Performance of the First Part of the Injector for the S-Band Test Facility at DESY*, Proceedings of the 1996 International Linac Conference, Geneva, Switzerland.

[11] V. E. Balakin and A. A. Mikhailichenko, *The Conversion System for Obtaining High Polarized Electrons and Positrons*, Preprint INP 79-85, 1979.

[12] K. Flöttmann, *Investigations Toward the Development of Polarized and Unpolarized High Intensity Positron Sources for Linear Colliders*, DESY-93-161, 1993.

[13] R. Brinkmann, *Optimization of a Final Focus System for Large Momentum Bandwidth*, DESY-M-90-14, 1990.

[14] R. Brinkmann, J. Pflger, V. Shiltsev, N. Vinokuro, P. Vobly, *Wiggler Options for TESLA Damping Ring*, DESY-TESLA-95-24, 1995.

[15] W. Nelson, H. Hirayama and D. Rogers, *The EGS4 Code System* SLAC-265, 1985.

[16] S. Ecklund, *Positron Target Materials Tests*, SLAC Collider Note-128, 1981.

[17] E. M. Reuter and J. A. Hodgson, *3D Nummerical Thermal Stress Analysis of the High Power Target for the SLC Positron Source*, SLAC-PUB-5370, 1991.

[18] R. H. Helm, *Adiabatic Approximation for Dynamics of a Particle in the Field of a Tapered Solenoid*, SLAC-4, 1962.

[19] H. Ida, *Present R&D Status of Positron Sources for JLC-1 and ATF*, presented at Sixth International Workshop on Linear Colliders, Tsukuba 1995.